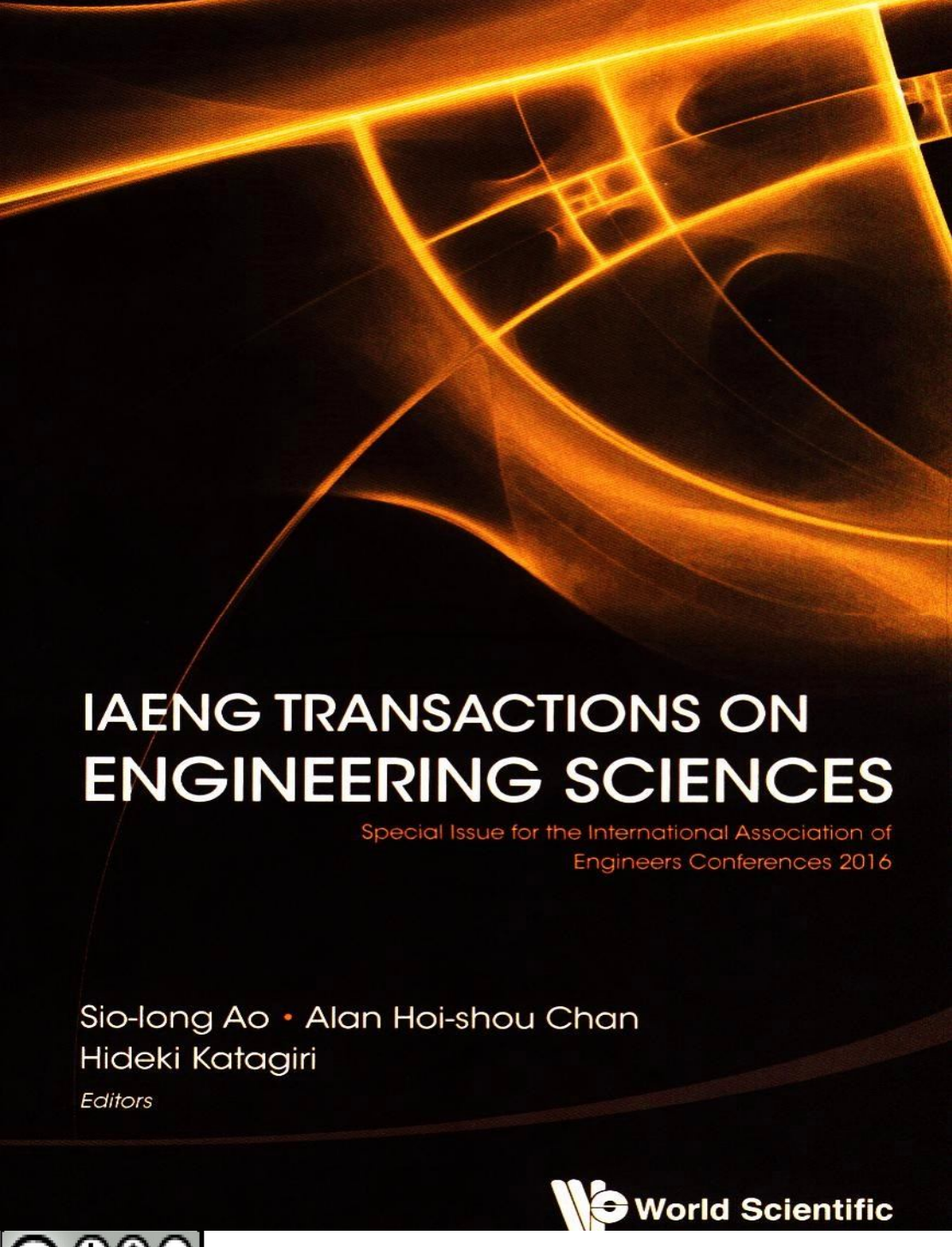

IAENG TRANSACTIONS ON ENGINEERING SCIENCES

Special Issue for the International Association of Engineers Conferences 2016

Editors

Sio-Iong Ao

International Association of Engineers, Hong Kong

Alan Hoi-shou Chan

City University of Hong Kong, Hong Kong

Hideki Katagiri

Kanagawa University, Japan

World Scientific

NEW JERSEY • LONDON • SINGAPORE • BEIJING • SHANGHAI • HONG KONG • TAIPEI • CHENNAI • TOKYO

Published by

World Scientific Publishing Co. Pte. Ltd.

5 Toh Tuck Link, Singapore 596224

USA office: 27 Warren Street, Suite 401-402, Hackensack, NJ 07601

UK office: 57 Shelton Street, Covent Garden, London WC2H 9HE

Library of Congress Cataloging-in-Publication Data

Names: Ao, Sio-Iong, editor. | Chan, Alan H. S., editor. | Katagiri, Hideki, editor. |
International Association of Engineers, sponsoring body. | International Multi-Conference of
Engineers and Computer Scientists (2016 : Hong Kong, China), author. |
World Congress on Engineering (2016 : London, England), author.

Title: Special issue for the International Association of Engineers conferences 2016 / edited by:
Sio-Iong Ao (International Association of Engineers, Hong Kong), Alan Hoi-shou Chan
(City University of Hong Kong, Hong Kong), Hideki Katagiri (Hiroshima University, Japan).

Description: New Jersey : World Scientific, [2017] | Series: IAENG transactions on engineering
sciences | Contains 21 revised papers from Hong Kong, March 16–18, 2016,
the International MultiConference of Engineers and Computer Scientists (IMECS 2016), and
London, UK, June 29–July 1, 2016, under the World Congress on Engineering (WCE 2016). |
Includes bibliographical references.

Identifiers: LCCN 2017017198 | ISBN 9789813226197 (hc : alk. paper)

Subjects: LCSH: Engineering--Congresses. | Computer science--Congresses.

Classification: LCC TA5 .S6642 2017 | DDC 620--dc23

LC record available at https://lccn.loc.gov/2017017198

British Library Cataloguing-in-Publication Data

A catalogue record for this book is available from the British Library.

Desk Editor: V. Vishnu Mohan

Typeset by Stallion Press
Email: enquiries@stallionpress.com

Printed in Singapore

CONTENTS

ENHANCED EFFICIENCY OF LARGE WIND POWER GENERATOR APPLICATIONS USING POWER FACTOR CONTROLLER MECHANISM

J. K. OBICHERE* and M. G. JOVANOVIC+

Department of Physics and Electrical Engineering, Northumbria University, Newcastle upon Tyne, NE1 8ST, UK
**judekennedyobichere@yahoo.com,*
+milutin.jovanovic@northumbria.ac.uk
www.northumbria.ac.uk

This work presents a vector control (VC) of an emerging brushless doubly-fed reluctance (BDFRG) technology for large wind turbine applications. The BDFRG has been receiving increasing attention due to its low operation and maintenance costs afforded by the use of partially-rated power electronics, and the high reliability of brushless assembly, while offering performance competitive to its traditional slip-ring counterpart, the doubly-fed induction generator (DFIG). A robust VC strategy has been developed for a custom-designed BDFRG fed from a conventional 'back-to-back' IGBT converter. Preliminary studies have evaluated the algorithm under the power factor control (PFC) conditions which allow the enhanced efficiency of the generator-converter set and the entire wind energy conversion systems (WECS).

Keywords: Brushless; Doubly-Fed Generators; Enhanced Efficiency; Power Factor Control; Vector Control; Wind Energy.

1. Introduction

The brushless doubly-fed generator (BDFG) has been considered as a viable replacement to the traditional DFIG for wind turbines [1]. In these applications, where only a limited variable speed capability is required (e.g. typically, in a 2:1 range or so [1, 4]), the BDFG should retain the DFIG economic benefits of using a relatively smaller inverter (e.g. around 25% of the machine rating), but with higher reliability and maintenance-free operation afforded by the absence of brush gear [5].

The BDFRG has two standard stator windings of different applied frequencies and pole numbers, unlike the DFIG. The primary (power) winding is grid-connected, and the secondary (control) winding is normally supplied from a bi-directional power converter. A BDFG reluctance type (Fig. 1), the brushless doubly-fed reluctance generator (BDFRG), appears to be more attractive than its 'nested' cage rotor form, the brushless doubly-fed induction generator (BDFIG) [6, 7]. This preference has been mainly attributed to the prospect for higher

efficiency [2] and simpler control associated with the cage-less reluctance rotor [8]. However, the BDFG rotor must have half the total number of stator poles to provide the rotor position dependent magnetic coupling between the stator windings required for the machine torque production.

With the recent introduction of the grid codes [9], another important BDFG merit is the superior low-voltage-fault-ride-through (LVFRT) capability to the DFIG [10–12]. It has been shown that owing to the larger leakage inductances and lower fault current levels, the LVFRT of the BDFIG may be accomplished safely without a crowbar circuitry [9, 13]. These potential LVFRT performance advantages over the DFIG can be carried over to the BDFRG featuring the leakage reactance values of the same order as the BDFIG.

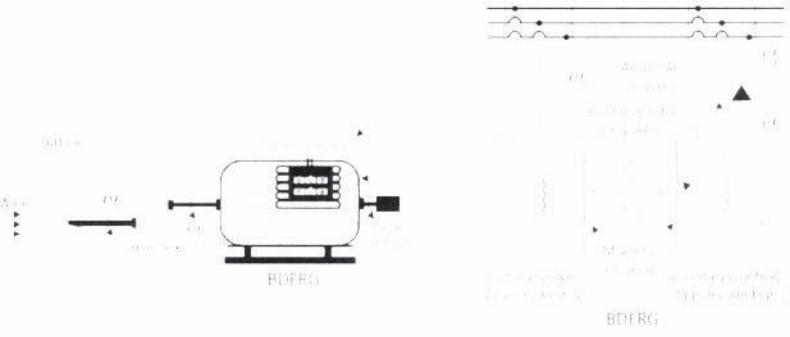

Fig. 1. Typical BDFRG drive set-up of variable speed WECS.

Various control algorithms have been developed for the BDFRG including scalar control [1], vector control (VC) [1, 17], direct torque control, torque and reactive power control [14], direct power control, sliding mode power control, field-oriented control [15], and even non-linear Lyapunov control theory. Although a comparative analysis of some of these control methods has been partly made in [15] (and more detailed for the DFIG in [10]), it is interesting that there is very little reported specifically on Power Factor Control (PFC) of the BDFRG being of utmost importance for generator applications [13]. In the BDFRG, the 'VC' term is commonly referred to as the primary winding voltage control, by analogy to the stator voltage control of the DFIG.

With a proper selection of the reference frames and careful tuning of the dedicated PI controllers, a very good potential and dynamic response of the VC scheme has been demonstrated without knowledge of any machine parameters. The VC performance is examined using the power factor control (PFC)

mechanism [14, 18–21] on a large, custom-built 2 MW BDFRG [4]. This control objective has been considered because of the achievable efficiency gain at unity line power factor. Extensive realistic simulation results taking into account the usual practical effects (e.g. transducers' DC offset, noise in measurements, and a PWM power converter model) are presented to support the discussions in this work.

2. Modeling and Operation of the BDFRG

The dynamic model of the BDFRG in arbitrary rotating reference frames, assuming motoring convention, can be represented using standard complex notation as [3]:

$$\left.\begin{aligned} \mathbf{v}_p &= R_p\mathbf{i}_p + \frac{d\boldsymbol{\lambda}_p}{dt} = R_p\mathbf{i}_p + \frac{d\boldsymbol{\lambda}_p}{dt}\Big|_{\theta_{p\,const}} + j\omega_p\boldsymbol{\lambda}_p \\ \mathbf{v}_s &= R_s\mathbf{i}_s + \frac{d\boldsymbol{\lambda}_s}{dt} = R_s\mathbf{i}_s + \frac{d\boldsymbol{\lambda}_s}{dt}\Big|_{\theta_{s\,const}} + j\omega_s\boldsymbol{\lambda}_s \\ \boldsymbol{\lambda}_p &= \underbrace{L_p i_{pd} + L_{ps} i_{sd}}_{\lambda_{pd}} + j.\underbrace{(L_p i_{pq} - L_{ps} i_{sq})}_{\lambda_{pq}} \\ \boldsymbol{\lambda}_s &= \lambda_{sd} + j.\lambda_{sq} = \sigma L_s\mathbf{i}_s + \underbrace{\frac{L_{ps}}{L_p}\boldsymbol{\lambda}_p^*}_{\lambda_{ps}} \end{aligned}\right\} \quad (1)$$

where the primary and secondary winding are denoted by the subscripts 'p' and 's' respectively, $\sigma = 1 - \frac{L_{ps}^2}{L_p L_s}$ is the leakage factor, and λ_{ps} is the primary flux linking the secondary winding (i.e. the mutual flux linkage).

The fundamental angular velocity and torque relationships for the machine with p_r rotor poles and $\omega_{p,s} = 2\pi f_{p,s}$ applied angular frequencies to the respective 2p-pole primary and 2q-pole secondary windings are [3]:

$$\omega_{rm} = \frac{\omega_p + \omega_s}{p_r} \leftrightarrow n_{rm} = 60.\frac{f_p + f_s}{p_r} \quad (2)$$

$$T_e = \frac{3p_r}{2}(\lambda_{p_{sd}} i_{sq} - \lambda_{p_{sq}} i_{sd}) \quad (3)$$

$$T_a = J.\frac{d\omega_{rm}}{dt} = T_e - T_L(\omega_{rm}) - F.\omega_{rm} \quad (4)$$

Notice that $\omega_s > 0$ for 'super-synchronous' operation, and $\omega_s < 0$ at sub-synchronous speeds (i.e. an opposite phase sequence of the secondary to the primary winding) in (2) where $\omega_{syn} = \frac{\omega_p}{p_r}$ is the synchronous speed (for $\omega_s = 0$ i.e. a DC secondary) as with a $2p_r$-pole wound rotor synchronous turbo-machine.

It is also worth mentioning that all the ω_p rotating vectors in the primary voltage/flux equations in (1) are in ω_p frame, whilst the corresponding secondary counterparts, including the λ_{qs} components in (3), are stationary in $p_r\omega_{rm} - \omega_p = \omega_s$ frame [3]. Given that λ_p and λ_{qs} in (3) are approximately constant by the primary winding grid connection, torque control can obviously be achieved through the secondary dq currents in the ω_s rotating frame.

Using (2), one can derive the mechanical power equation indicating individual contributions of each BDFRG winding:

$$P_m = T_e.\omega_{rm} = \underbrace{\frac{T_e.\omega_p}{p_r}}_{P_p} + \underbrace{\frac{T_e.\omega_s}{P_r}}_{P_s} = P_p.\left(1 + \frac{\omega_s}{\omega_p}\right) \tag{5}$$

The machine operating mode is determined by the power flow in the primary winding i.e. to the grid for the generating ($T_e < 0$) regime under consideration, while the secondary winding can either take or deliver real power (P_s) subject to its phase sequence i.e. the ω_s sign; the BDFRG would absorb (produce) $P_s > 0$ at sub- or super-synchronous speeds.

3. Controller System Design

The detailed BDFRG system layout with a generic controller design is presented in Fig. 2. A standard phase-locked-loop (PLL) algorithm, readily available in the *Simulink* library, has been used to retrieve the stationary α-β frame angular positions (θ/θ_p) of the primary voltage/flux vectors from the measured voltages and/or currents. Furthermore, a conventional vector controller with space-vector PWM of the active rectifier has been implemented for control of DC link voltage and unity line power factor [13, 18-20]. The primary real (P) and reactive (Q) power calculations are reference frame invariant and have been done using the stationary frame voltages ($v_{\alpha\beta}$) and currents ($i_{\alpha\beta}$) to avoid unnecessary conversions into their rotating d_s-q_s equivalents, and the use of time-consuming trigonometric functions, allowing so the higher control rates and superior performance in practice. The Q reference is often set to zero ($Q^* = 0$) for the unity primary power factor but can be any other value of interest for a given real power setting (P^*) in power control mode, or the desired angular velocity ω^*_{rm} in variable speed systems. For example, either P^* or ω^*_{rm} may correspond to the Optimum Power Point Tracking (OPPT) of a wind turbine [1], while Q^* was chosen to optimize efficiency of the WECS in this paper.

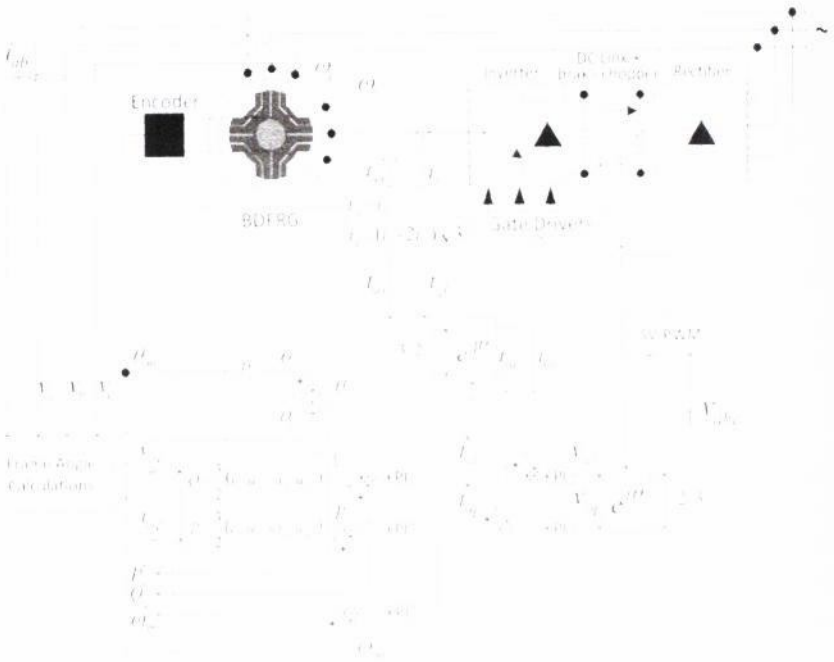

Fig. 2. Structural diagram of the BDFRG drive set-up.

4. Voltage Control (VC) System

The control form expressions can be derived from the BDFRG space-vector model (1) in the natural reference frames, ω_p (i.e. d_p-d_q for the primary winding) and ω_s (i.e. d_s-q_s for secondary winding) rotating frames (Fig. 3), where the respective vector components appear as DC quantities. Substituting for $\mathbf{i}_p$ from the λ_p equation of (1) into $\mathbf{S}_p = \frac{3}{2}\mathbf{v}_p\mathbf{i}_p^*$ would lead to the following relationships for the primary mechanical and reactive power:

$$P_p = \frac{3}{2}\omega_p(\lambda_{p_{sd}} i_{sq} - \lambda_{p_{sq}} i_{sd}) \tag{6}$$

$$Q_p = \frac{3}{2}\omega_p\left(\frac{\lambda_p^2}{L_p} - \lambda_{p_{sd}} i_{sd} - \lambda_{p_{sq}} i_{sq}\right) \tag{7}$$

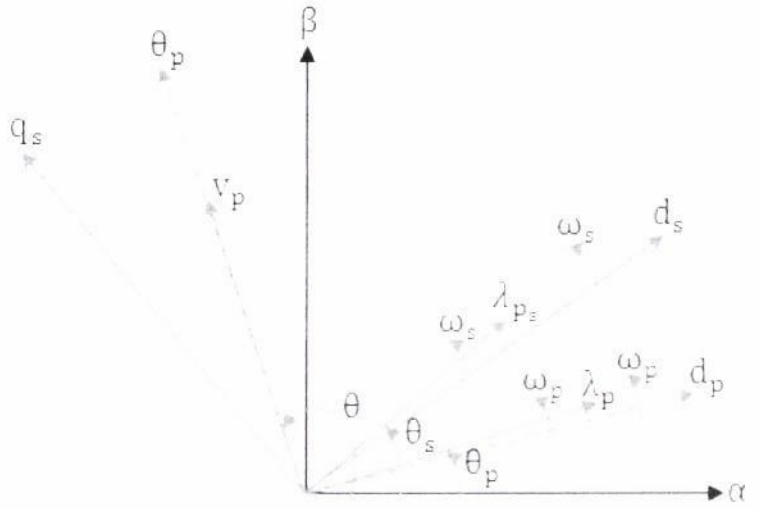

Fig. 3. Identification of primary voltage flux vectors in a stationary α-β reference frame.

A trade-off of the machine parameter independence is that VC of P_p and Q_p is coupled as both the i_{sd} and i_{sq} secondary current components appear in (6) and (7). The level of this cross-coupling can be reduced by aligning the q_p-axis of the reference frame to the primary voltage vector as shown in Fig. 3. In this case the primary flux vector (λ_p), would be phase-shifted ahead of the corresponding d_p-axis depending on the winding resistance values which are getting smaller with larger machines. Therefore, for the frame alignment choice as in Fig. 3, $\lambda_{p_{sd}} \gg \lambda_{p_{sq}}$ i.e. $\lambda_{p_{sd}} \approx \lambda_{ps}$ so that the approximations of (6) and (7) become:

$$P_p \approx \frac{3}{2}\omega_p\lambda_{ps}i_{sq} = \frac{3}{2}\frac{L_{ps}}{L_p}\omega_p\lambda_p i_{sq} \tag{8}$$

$$Q_p \approx \frac{3}{2}\frac{\omega_p\lambda_p^2}{L_p} - \frac{3}{2}\omega_p\lambda_{ps}i_{sd} \tag{9}$$

$$= \frac{3}{2}\frac{\omega_p\lambda_p}{L_p}\left(\lambda_p - L_{ps}i_{sd}\right) = \frac{3}{2}\omega_p\lambda_p i_{pd} \tag{10}$$

The P_p vs i_{sq} and Q_p vs i_{sd} functions above are nearly linear, which justifies the use of PI controllers in Fig. 2. Therefore, all inductance variations in (9)-(12) can be effectively taken care of by optimal tuning of the PI gains so their prior knowledge is not required for control purposes.

5. PF Operating Principle of the BDFRG Wind Turbine

The preliminary performance of the VC scheme in Fig. 2 has been assessed using the parameters of a large-scale BDFRG [4, 16] in Table 1 for simulation studies. In order to make the simulations as realistic as possible, the following actions have been taken and/or assumptions made: (i) The power electronic models from the *SimPowerSystems* toolbox have been implemented; (ii) High-frequency uncorrelated white noise and unknown slowly varying DC offset have been superimposed to the ideal signals to account for practical effects of the measurement noise and current/voltage transducers errors; (iii) Finally, the rotor position and speed information has been provided by a shaft sensor.

In a typical WECS, the turbine torque on the generator side of the gear-box for the maximum wind energy extraction in the base speed region (i.e. between the minimum 'cut-in', u_{min}, and the rated wind speed, u_r), can be represented as [1, 5]:

$$T_{opt} = \frac{A.\rho.C_p(\lambda_{opt},\gamma).R^3}{2.g^3.\lambda_{opt}^3}.\omega_{rm}^2 = K_{opt}.\omega_{rm}^2 \qquad (11)$$

where ρ is the air density, $C_p(\lambda,\gamma)$ is the power coefficient (i.e. the maximum turbine efficiency as $\lambda = \lambda_{opt}$ in this case), $\lambda_{opt} = \frac{R\omega_t}{u}$ is the optimum tip speed ratio for a given wind speed u, ω_t is the turbine rotor angular velocity, γ is the pitch angle (normally fixed to zero to maximize C_p), R the radius of the circular swept area ($A = \pi R^2$), and $g = \frac{\omega_{rm}}{\omega_t}$ is the gear ratio. The shaft torque-speed profile in (4) is of the same form as (11):

$$T_L = -\frac{P_r}{\omega_r}.\left(\frac{n_{rm}}{n_{max}}\right)^2 \approx -19.\left(\frac{n_{rm}}{1000}\right)^2 \text{ kNm} \qquad (12)$$

Table1. The BDFRG design specifications.

Symbol	Quantity	Values & Units
J	Rotor inertia	3.8kgm^2
R_p	Primary resistance	0.0375 Ω
R_s	Secondary resistance	0.0575 Ω
L_p	Primary inductance	1.17mH
L_s	Secondary inductance	2.89mH
$L_{p,s}$	Mutual inductance	0.98mH
p_r	Rotor poles	4
P	Primary power	2 MW
n_r	Rated speed	1000 rev/min
$I_{p,s}$	Stator currents	1.5kArms
V_p	Primary voltage	690Vrms
f_p	Supply frequency	50 Hz
Y/Y	Winding connections	-
p/q	Stator poles	6/2

6. Simulation Outcome

The simulation results in Figs. 4-9 have been produced by running the control algorithms in Fig. 2 at 5 kHz switching rate for the IGBT converter. The DC link voltage has been maintained at ≈ 1200 V by the PWM rectifier (i.e. the line-side bridge) supplied at 690 V, 50 Hz. The reference speed trajectory is set as a steep ramp signal suited for dynamically not very demanding wind power applications even under extreme turbulent wind conditions.

The top plots in Fig. 4 show the excellent speed tracking with no overshoot following the start-up period in both super- and sub-synchronous modes of the BDFRG over the limited speed range of 600-900 rpm. The primary electrical power (P) and electro-magnetic torque (T_e) curves reflect (12) for the specific speed settings. Except for a difference in losses, and considering that $\omega_p \approx$ const, P and T_e are directly related as follows from (5) and (6) which explains a close resemblance in their shape. The T_e deviations from the desired profile during the speed transients refer to the acceleration or deceleration torque term in (4) depending on whether the machine is to speed-up ($T_a > 0$) or slow-down ($T_a < 0$). The reasonably accurate and smooth $Q_p \approx 0$ control can be observed to be little affected by the variable speed dependent loading disturbances, which means that the optimum power factor control (OPFC) conditions have been largely met. Note that the outer PI speed control loop is required to ensure effective variable speed operation at optimum tip-speed ratio.

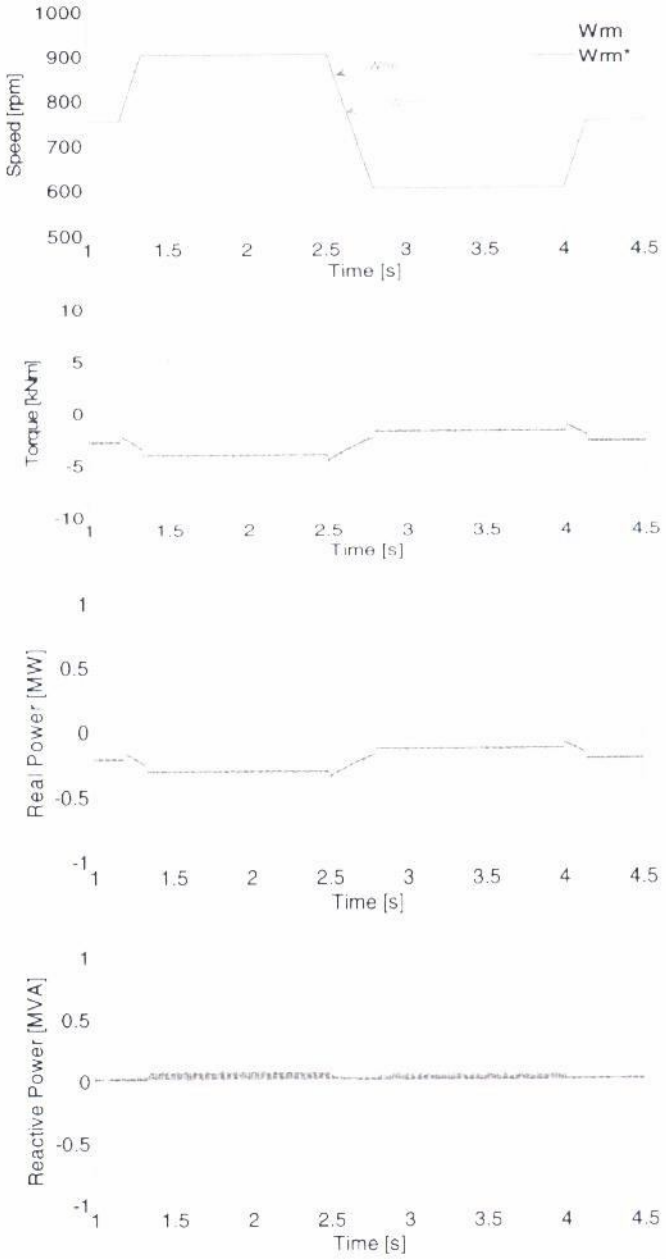

Fig. 4. PF performance of BDFRG in a limited range at synchronous speed (750 rpm).

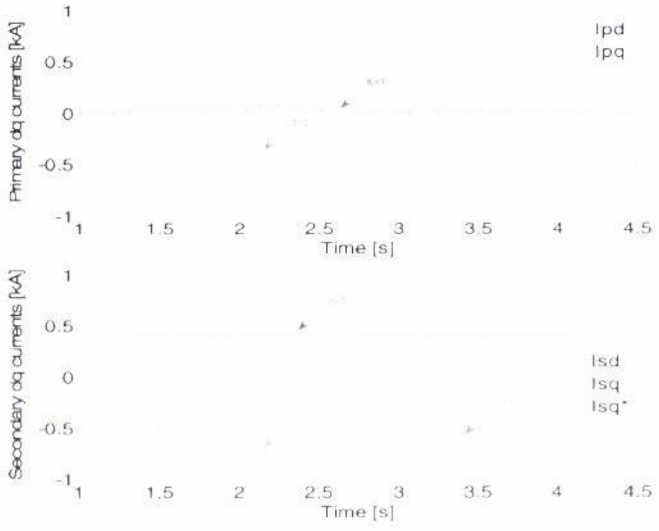

Fig. 5. PF responses of BDFRG current components in the rotating reference frames.

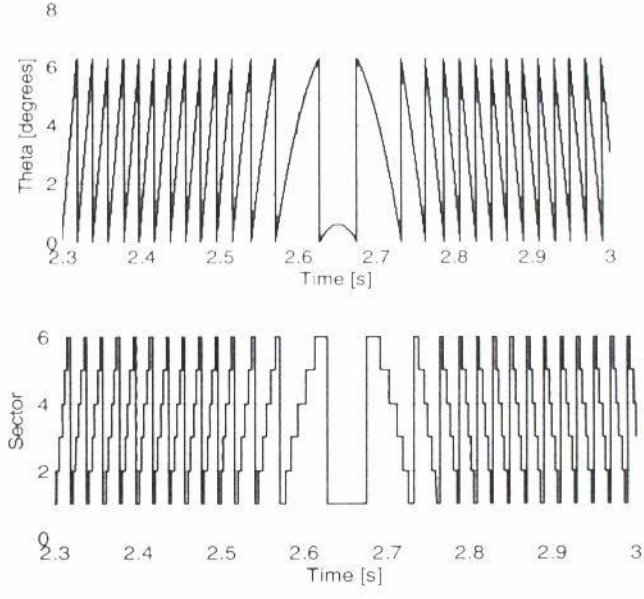

Fig. 6. PWM space Sectors, angular (theta) positions and switching times of active voltage vectors of BDFRG showing phase sequence reversal during the speed mode transition at unity power factor.

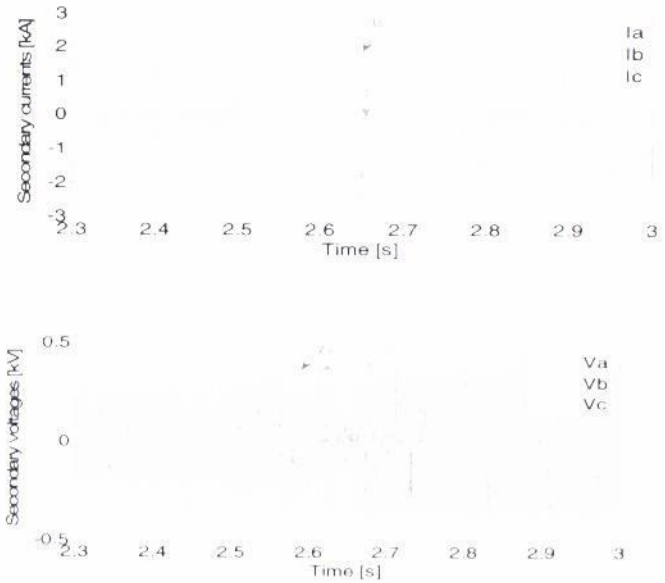

Fig. 7. BDFRG angular (theta) positions and secondary voltage waveforms showing a phase sequence reversal during the speed mode transition at unity power factor.

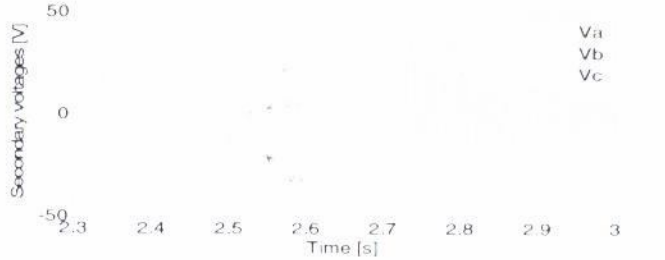

Fig. 8. Enhanced BDFRG secondary voltage waveforms showing a phase sequence reversal during the speed mode transition at unity power factor.

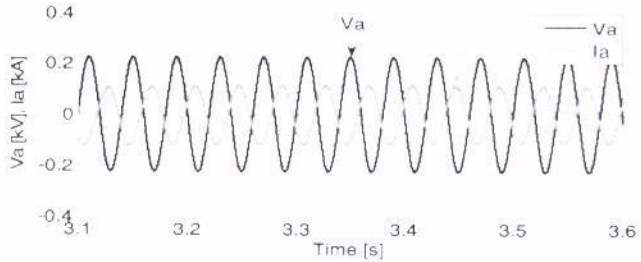

Fig. 9. Primary voltage and current at unity power factor.

The secondary ($i_{sd,q}$) and primary ($i_{pd,q}$) current waveforms in Fig. 5 show no transient over-currents as the PI regulators do not need to be saturated to allow accurate tracking of the desired trajectories for the moderate ramp speed variations. A close link between the active q currents and the real power (torque), as well as the magnetizing d currents and Q, is immediately visible from the respective waveforms. The coupling effects of the i_{sq} clearly manifest themselves as speed (torque) dependent disturbance (e.g. offsets) in the respective non-controllable i_{pd} profiles by analogy to the P and Q scenario in Fig. 4.

Figure 6 illustrates the step-wise PWM angular positions of the modulated secondary voltage vector (v_s), and the respective space sector variations, while Fig. 7 shows the respective secondary currents and voltages, during a speed reduction, from 900 rev/min. to 600 rev/min. That is, the speed mode change, from super- to sub-synchronous. In the super-synchronous mode, v_s rotates anti-clockwise as indicated by the ascending angular steps for the same phase sequence of the windings and $\omega_s > 0$ in (2). The situation is reversed at sub-synchronous speeds when v_s rotates clockwise with the angular steps descending, which comes from the opposite phase sequence of the secondary to the primary winding since $\omega_s < 0$ in (2). Notice that v_s becomes stationary at synchronous speed as the secondary currents are then DC i.e. $\omega_s = 0$ in (2).

Figure 8 shows the enhanced secondary voltage while Fig. 9 shows the respective phase voltage and current waveforms which are π-rad out of phase as expected for unity power factor control (-1 in generating mode) in steady-state period.

7. Conclusions and Perspectives

A novel power factor control (PFC) mechanism for enhanced efficiency of the BDFRG has been carried out and evaluated by comprehensive simulation studies under typical operating conditions. Such vector control implementation can serve as a platform for further research on this emerging and prominent brushless machine topology for applications in large wind turbines and industries, where the cost advantages of partially-rated power electronics and high reliability of brushless structure can be fully utilized.

The enhanced simulation works in Matlab®/Simulink® have clearly demonstrated the immense potential and effectiveness of the controller(s) using the power factor control mechanism. The presented results are more than encouraging and can serve as basis for further research work on this machine.

References

1. M. G. Jovanovic, R. E. Betz and J. Yu, *The use of doubly fed reluctance machines for large pumps and wind turbines*, IEEE Transactions on Industry Applications, vol. 38, pp. 1508–1516, 2002.
2. F. Wang, F. Zhang and L. Xu, *Parameter and performance comparison of doubly-fed brushless machine with cage and reluctance rotors*, IEEE Transactions on Industry Applications, vol. 38, no. 5, pp. 1237–1243, 2002.
3. R. E. Betz and M. G. Jovanovic, *Introduction to the space vector modeling of the brushless doubly-fed reluctance machine*, Electric Power Components and Systems, vol. 31, no. 8, pp. 729–755, 2003.
4. D. G. Dorrell and M. Jovanovic, On the possibility of using a brushless doubly-fed reluctance generator in a 2 MW wind turbine, *IEEE Industry Applications Society Annual Meeting* pp. 1–8, 2008.
5. H. Polinder, F. Van der Pijl, G. de Vilder and P. Tavner, *Comparison of direct-drive and geared generator concepts for wind turbines*, IEEE Transactions on Energy Conversion, vol. 21, no. 3, pp. 725–733, 2006.
6. S. Tohidi, M. Zolghadri, H. Oraee, P. Tavner, E. Abdi and T. Logan, *Performance of the brushless doubly-fed machine under normal and fault conditions*, IET Electric Power Applications, vol. 6, no. 9, pp. 621–627, 2012.
7. F. Barati, R. McMahon, S. Shao, E. Abdi and H. Oraee, *Generalized vector control for brushless doubly fed machines with nested-loop rotor*, IEEE Transactions on Industrial Electronics, vol. 60, no. 6, pp. 2477–2485, 2013.
8. A. Knight, R. Betz and D. Dorrell, *Design and analysis of brushless doubly fed reluctance machines*, IEEE Transactions on Industry Applications, vol. 49, no. 1, pp. 50–58, 2013.
9. T. Long, S. Shao, P. Milliband, E. Abdi and R. McMahon, *Crowbarless fault ride-through of the brushless doubly fed induction generator in a wind turbine under symmetrical voltage dips*, IEEE Transactions on Industrial Electronics, vol. 60, no. 7, pp. 2833–2841, 2013.
10. R. Cardenas, R. Pena, S. Alepuz and G. Asher, *Overview of control systems for the operation of DFIGs in wind energy applications*, IEEE Transactions on Industrial Electronics, vol. 60, no. 7, pp. 2776–2798, 2013.
11. G. Marques and D. Sousa, *Understanding the doubly fed induction generator during voltage dips*, IEEE Transactions on Energy Conversion, vol. 27, no. 2, pp. 421–431, 2012.
12. S. Tohidi, P. Tavner, R. McMahon, H. Oraee, M. Zolghadri, S. Shao and E. Abdi, *Low voltage ride-through of DFIG and brushless DFIG:*

Similarities and differences, Electric Power Systems Research, vol. 110, no. 10, pp. 64–72, 2014.

13. Jude K. Obichere, Milutin Jovanovic and Sul Ademi, *Power Factor Control of Large Doubly-Fed Reluctance Wind Generators*, Lecture Notes in Engineering and Computer Science: Proceedings of The World Congress on Engineering and Computer Science 2015, WCECS 2015, 21 23 October, 2015, San Francisco, USA, pp. 210–215.
14. H. Chaal and M. Jovanovic, *Practical Implementation of sensorless torque and reactive power control of doubly fed machines*, IEEE Transactions on Industrial Electronics, vol. 59, no. 6, pp. 2645–2653, 2012.
15. S. Ademi, M. Jovanovic and J. K. Obichere, *Comparative analysis of control strategies for large doubly-fed reluctance wind generators*, Lecture Notes in Engineering and Computer Science: Proceedings of The World Congress on Engineering and Computer Science 2014, WCECS 2014, 22–24 October, 2014, San Francisco, USA, pp. 245–250.
16. S. Ademi and M. Jovanovic, *Control of emerging brushless doubly fed reluctance wind turbine generators*, in large scale renewable power generation, series on Green Energy and Technology, eds. J. Hossain and A. Mahmud (Springer, Singapore, 2014), pp. 395–411.
17. Milutin Jovanovic, Sul Ademi and Jude K. Obichere, *Comparisons of Vector Control Algorithms for Doubly-Fed Reluctance Wind Generators*, Transactions on Engineering Technologies, World Congress on Engineering and Computer Science 2014, eds. Haeng Kon Kim, Mahyar A. Amouzegar and Sio-long Ao (Springer, Dordrecht, 2015) pp. 85–99.
18. Jude K. Obichere, Milutin Jovanovic and Sul Ademi, *Power Factor Control of Large Doubly-Fed Reluctance Wind Generators*, Lecture Notes in Engineering and Computer Science 2015, WCECS 2015, 21 23 October, 2015, San Francisco, USA, pp. 210–215.
19. Jude K. Obichere, Milutin Jovanovic and Sul Ademi, *Improved Power Factor Controller for Wind Generator and Applications*, Engineering Letters, vol. 24, no. 2, pp. 125–131, 2016.
20. Jude K. Obichere and Milutin Jovanovic, *Optimum Power Factor Control of Large Doubly-Fed Reluctance Wind Generator Applications*, Lecture Notes in Engineering and Computer Science: Proceedings of The World Congress on Engineering 2016, WCE 2016, 29 June–1 July, 2016, London, U. K., pp. 291–296.
21. S. Ademi and M. Jovanovic, *Vector control methods for brushless doubly fed reluctance machines*, IEEE Transactions on Industrial Electronics, vol. 62, no. 1, pp. 96–104, 2015.